Numerical and analytical modeling of the end-loaded split (ELS) test specimens made of multi-directional coupled composite laminates

Sylwester Samborski, and Paolo S. Valvo

Citation: AIP Conference Proceedings **1922**, 030003 (2018);
View online: https://doi.org/10.1063/1.5019037
View Table of Contents: http://aip.scitation.org/toc/apc/1922/1
Published by the American Institute of Physics

Numerical and Analytical Modeling of the End-Loaded Split (ELS) Test Specimens Made of Multi-Directional Coupled Composite Laminates

Sylwester Samborski[1, a)] and Paolo S. Valvo[2, b)]

[1]*Faculty of Mechanical Engineering, Lublin University of Technology, Nadbystrzycka 36, 20-618 Lublin, Poland*
[2]*Department of Civil and Industrial Engineering, University of Pisa, Largo Lucio Lazzarino, I-56122 Pisa (PI), Italy*

[a)]Corresponding author: s.samborski@pollub.pl
[b)]p.valvo@ing.unipi.it

Abstract. The paper deals with the numerical and analytical modelling of the end-loaded split test for multi-directional laminates affected by the typical elastic couplings. Numerical analysis of three-dimensional finite element models was performed with the Abaqus software exploiting the virtual crack closure technique (VCCT). The results show possible asymmetries in the widthwise deflections of the specimen, as well as in the strain energy release rate (SERR) distributions along the delamination front. Analytical modelling based on a beam-theory approach was also conducted in simpler cases, where only bending-extension coupling is present, but no out-of-plane effects. The analytical results matched the numerical ones, thus demonstrating that the analytical models are feasible for test design and experimental data reduction.

INTRODUCTION

Multi-directional (MD) laminates made of several layers of variously oriented fiber-reinforced polymer (FRP) laminae, or plies, offer great advantages in many engineering applications from aircraft to marine and automotive industries, as they enable tailoring the structural response to specific design needs. Nonetheless, the widespread use of such structural components is hindered by the requirement of more complex analysis tools with respect to unidirectional (UD) laminates [1], as well as by a poor understanding of the related damage mechanisms and failure modes [2], as testified by the lack of standard testing procedures for the delamination toughness of MD laminates [3].

Modelling difficulties for multi-directional laminates include the presence of elastic couplings between the extension, bending, shear, and torsion deformations and the corresponding internal forces and moments [4, 5]. Moreover, like composite structures in general, they are prone to damage phenomena, such as delamination [6, 7, 8].

In previous studies, theoretical calculations and experiments concerning different delamination fracture modes have been performed for different loads and boundary conditions for laminated beams [9, 10]. The main goal was to recognize the influence of a general ply lay-up with different mechanical couplings and boundary conditions on the actual distribution of fracture toughness along the delamination front with different ply angles at interfaces. The current work covers analyses of the end loaded split (ELS) test configuration (Fig. 1), defined in the ISO 15114 Standard for unidirectional laminates [11].

Local discrepancies in the stress/strain fields coming from different interfacial fiber-angles generate uneven deformations of the specimens' legs and, consequently, affect the strain energy release rate (SERR) distribution along the delamination front. In general, mixed-mode fracture conditions should be expected [12], so that the adopted fracture criterion should allow for each of the three main fracture modes to be determined and properly considered.

Computer Methods in Mechanics (CMM2017)
AIP Conf. Proc. 1922, 030003-1–030003-8; https://doi.org/10.1063/1.5019037
Published by AIP Publishing. 978-0-7354-1614-7/$30.00

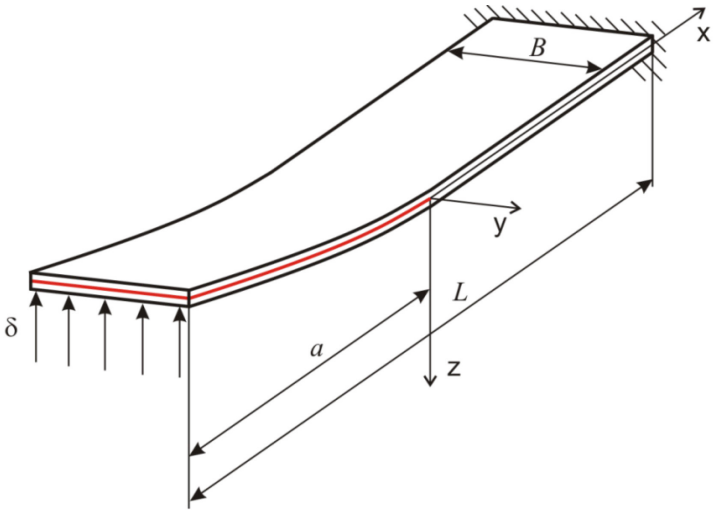

FIGURE 1. Configuration of the ELS test specimen

MECHANICAL COUPLINGS IN LAMINATES

According to classical lamination theory (CLT) [8], the internal force, $\mathbf{N} = [N_x, N_{xy}, N_{xy}]^T$, and moment, $\mathbf{M} = [M_x, M_{xy}, M_{xy}]^T$, vectors are related to the strain measures as follows [10]:

$$\begin{Bmatrix} N_x \\ N_y \\ N_{xy} \end{Bmatrix} = \mathbf{A}\begin{Bmatrix} \varepsilon_x^0 \\ \varepsilon_y^0 \\ \gamma_{xy}^0 \end{Bmatrix} + \mathbf{B}\begin{Bmatrix} \kappa_x^0 \\ \kappa_y^0 \\ \kappa_{xy}^0 \end{Bmatrix}, \quad \begin{Bmatrix} M_x \\ M_y \\ M_{xy} \end{Bmatrix} = \mathbf{B}\begin{Bmatrix} \varepsilon_x^0 \\ \varepsilon_y^0 \\ \gamma_{xy}^0 \end{Bmatrix} + \mathbf{D}\begin{Bmatrix} \kappa_x^0 \\ \kappa_y^0 \\ \kappa_{xy}^0 \end{Bmatrix} \tag{1}$$

where ε_x^0, ε_y^0, γ_{xy}^0 and κ_x^0, κ_y^0, κ_{xy}^0 are the strains and curvatures, respectively, of the laminate's mid-plane; **A**, **B**, and **D**, respectively are the extensional, coupling, and bending stiffness matrices. By denoting with $\bar{Q}_{ij}^k$ the elements of the elastic moduli matrix of the *k*-th ply (i, j =1...3), with z_k the distances of the ply surfaces from the mid-plane, and with *n* the total number of plies, the elements of the stiffness matrices are:

$$A_{ij} = \sum_{k=1}^{n} \bar{Q}_{ij}^k \left(z_k - z_{k-1}\right) \tag{2}$$

$$B_{ij} = \frac{1}{2}\sum_{k=1}^{n} \bar{Q}_{ij}^k \left(z_k^2 - z_{k-1}^2\right) \tag{3}$$

$$D_{ij} = \frac{1}{3}\sum_{k=1}^{n} \bar{Q}_{ij}^k \left(z_k^3 - z_{k-1}^3\right) \tag{4}$$

Note, that each of the matrices **A** and **D** can only have two forms, reflecting the presence or absence of the in-plane couplings. On the contrary, the out-of-plane coupling stiffness matrix **B** takes one of the six different coupled forms: $\mathbf{B}_L$, $\mathbf{B}_T$, $\mathbf{B}_{LT}$, $\mathbf{B}_S$ and $\mathbf{B}_F$ and the uncoupled one $\mathbf{B}_0$ [5]. This generates a great number of coupled layups and shows the extent of the unexplored field of coupled laminates mechanical properties.

FEM CALCULATIONS

The calculations of the laminated specimen model were performed using the finite element method (FEM). Three-dimensional FEM models of the ELS test specimens made of coupled laminates were analyzed with the commercial software Abaqus [15]. The beam model was built of the S4 and S4R shell elements (11 280 in total). The mesh was densified at the beam model edges, as well as in the prospective propagation area (cf. [9]), such that the mesh size was 0.5 and 2.5 mm. This enabled both high accuracy of the results and a reasonable computation time. The model was constructed by joining together two 3D shell beams with proper contact definition and a crack (delamination) embedded in the mid-plane. The boundary conditions (BCs) fulfilled the assumptions of the ELS test configuration – the non-delaminated end of the beam was fixed, such that no rotation nor translation was possible. The split end was loaded with the displacement δ (Fig. 1) in a quasi-static way - at ca. 0.5 mm/min. The complexity of the FE model and the computational task can be reflected by a number of degrees of freedom (DOFs) equal 82 026. The stress state and strain energy release rate along the initial delamination front were determined based on linear elastic fracture mechanics (LEFM) [14]. Simulations of the ELS test in the case of coupled laminates enabled distinction of the most problematic couplings from the point of view of a proper calculation of SERR in accordance with the ISO 15114 Standard [11].. Analyses were conducted up to initiation of delamination in accordance with the Benzeggagh-Kennane fracture criterion [16], implemented through the virtual crack closure technique (VCCT) [17]. The crack (delamination) was embedded in the model's mid-plane, i.e. between the two joined shell beams in ofder to fulfill the demands of the VCCT. In the propagation area, a set of node pairs was defined; these were subsequently separated across the x-y plane to simulate delamination expansion.

ANALYTICAL CALCULATIONS

In simpler cases, where no out-of-plane effects are present, an analytical approach is also pursued. The energy release rate and its modal contributions are calculated based on a simplified beam-theory model, which however accounts for bending-extension coupling [12]. Accordingly, the delaminated plate is considered as the assemblage of three sublaminates, which are rigidly connected to each other at the crack-tip cross section (Fig. 2a). Each sublaminate is modelled as an equivalent homogeneous Timoshenko beam in the *xz*-plane. Their extensional, coupling, shear, and bending stiffnesses are denoted with A_α, B_α, C_α, and D_α, respectively (Fig. 2b). Here and in the following, the subscripts $\alpha = 1$ and $\alpha = 2$ refer to the upper and lower sublaminates, respectively; $\alpha = 3$ refers to the (unbroken) base laminate. Besides, let H_α and h_α denote the sublaminate thickness and half thickness, respectively.

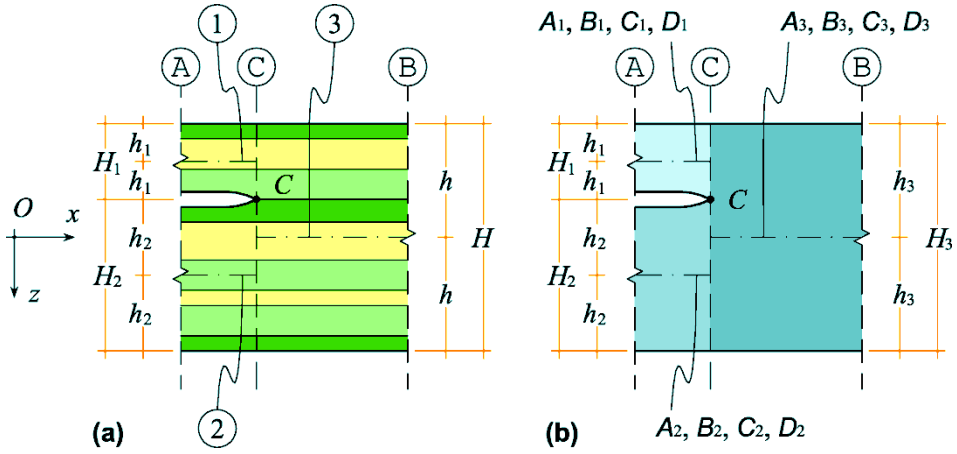

FIGURE 2. Crack-tip segment: (a) laminated beam; (b) assemblage of equivalent homogeneous beams

The adopted approach is based on the introduction of the crack-tip displacement rates,

$$\rho_u = \lim_{\Delta a \to 0} \frac{\Delta u}{\Delta a}, \quad \rho_w = \lim_{\Delta a \to 0} \frac{\Delta w}{\Delta a}, \quad \text{and} \quad \rho_\phi = \lim_{\Delta a \to 0} \frac{\Delta \phi}{\Delta a}, \tag{5}$$

defined as the relative displacements at the crack-tip per unit increase in crack length [18]. In turn, such quantities can be expressed as functions of the internal forces, N_1, Q_1, M_1 and N_2, Q_2, M_2, in the upper and lower sublaminates at the crack-tip cross section:

$$\begin{aligned} \rho_u &= \frac{1}{B}[(a_1 + b_1 h_1)N_1 - (a_2 - b_2 h_2)N_2 + (b_1 + d_1 h_1)M_1 - (b_2 - d_2 h_2)M_2], \\ \rho_w &= \frac{1}{B}(c_1 Q_1 - c_2 Q_2), \quad \text{and} \quad \rho_\phi = \frac{1}{B}(b_1 N_1 - b_2 N_2 + d_1 M_1 - d_2 M_2). \end{aligned} \tag{6}$$

In Eq. (6), the extensional, bending-extension coupling, shear, and bending compliances have been introduced:

$$a_\alpha = \frac{D_\alpha}{A_\alpha D_\alpha - B_\alpha^2}, \quad b_\alpha = -\frac{B_\alpha}{A_\alpha D_\alpha - B_\alpha^2}, \quad c_\alpha = \frac{1}{C_\alpha}, \quad \text{and} \quad d_\alpha = \frac{A_\alpha}{A_\alpha D_\alpha - B_\alpha^2}. \tag{7}$$

Thus, the energy release rate can be calculated as

$$G = \frac{1}{2B}\left[\frac{f_{\phi M}\rho_u^{\,2} - (f_{\phi N} + f_{uM})\rho_u \rho_\phi + f_{uN}\rho_\phi^{\,2}}{f_{uN} f_{\phi M} - f_{\phi N} f_{uM}} + \frac{\rho_w^{\,2}}{f_{wQ}}\right], \tag{8}$$

where

$$\begin{aligned} f_{uN} &= \frac{1}{B}(a_1 + a_2 + 2b_1 h_1 - 2b_2 h_2 + d_1 h_1^2 + d_2 h_2^2), \quad f_{uM} = f_{\phi N} = \frac{1}{B}(b_1 + b_2 + d_1 h_1 - d_2 h_2), \\ f_{wQ} &= \frac{1}{B}(c_1 + c_2), \quad \text{and} \quad f_{\phi M} = \frac{1}{B}(d_1 + d_2) \end{aligned} \tag{9}$$

are flexibility coefficients. Under I/II mixed-mode fracture conditions, the energy release rate is the sum of two contributions, $G = G_{\mathrm{I}} + G_{\mathrm{II}}$, related to fracture modes I and II, respectively. Based on the adopted model, these are:

$$G_{\mathrm{I}} = \frac{1}{2B}\left[\frac{1}{f_{uN}}\frac{(f_{uN}\rho_\phi - f_{\phi N}\rho_u)^2}{f_{uN} f_{\phi M} - f_{uM} f_{\phi N}} + \frac{\rho_w^2}{f_{wQ}}\right] \quad \text{and} \quad G_{\mathrm{II}} = \frac{1}{2B}\frac{\rho_u^2}{f_{uN}}. \tag{10}$$

In order to apply the general theory to the investigated case, it will be sufficient to notice that in an ELS test specimen the internal forces in the upper and lower sublaminates at the crack-tip cross section are:

$$\begin{aligned} N_1 &= 0, \quad Q_1 = \frac{P}{1+\beta}, \quad \text{and} \quad M_1 = Q_1 a; \\ N_2 &= 0, \quad Q_2 = \frac{\beta P}{1+\beta}, \quad \text{and} \quad M_2 = Q_2 a. \end{aligned} \tag{11}$$

where

$$\beta = \frac{c_1 + \frac{1}{3}d_1 a^2}{c_2 + \frac{1}{3}d_2 a^2} \tag{12}$$

is a coefficient used to share the total applied shearing load, P, between the upper and lower sublaminates. Hence, through Eqs. (6)-(10) all the quantities of interest can be easily calculated.

RESULTS AND DISCUSSION

In this section a comparison of the analytical and the numerical outcomes is provided. In Fig. 3 variability of the delamination-onset load along with the fiber angle in the bending-extension angle is presented. Both approaches – 2D analytical and 3D numerical seem to give similar results, even though the analytical values of P_c are higher by ca. 10%. Comparison of the phase angle values for different fiber angles (Fig. 3) shows practically no influence of the reinforcement direction (providing, the sequence induces the B-E coupling) on the values of ψ. Again, the numerical and the analytical results are very close with a slight predominance of the latter, in this case.

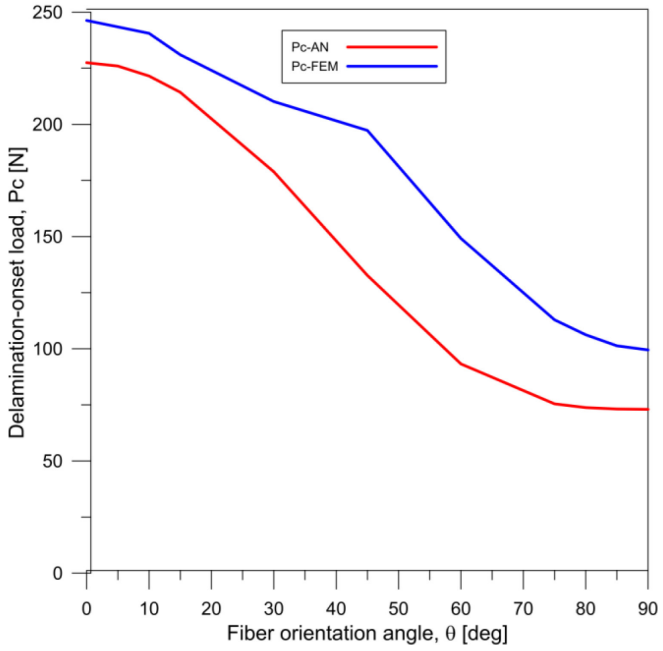

FIGURE 3. Variability of delamination-onset load for the ELS laminated beam with bending-extension coupling

Concerning the mode I strain energy release rate, G_I for different fiber angles (Fig. 4), there is more discrepancy between the two methods, especially for $\theta > 70°$; the FEM curve is the very steep what can be a manifestation of the difference in the 3D approach in relation to the 2D one. This effect is even stronger in Fig. 5, where the analytical and the FEM results differ significantly. The values of G_T are obviously very close to G_{II} which yields from the very nature of the ELS test, conceived for the mode II critical SERR determination – consider the very small values of G_I (Fig. 4) compared to G_T. Note also, that the analytical value of G_T is practically equal to the assumed material characteristic G_{IIc}, irrespectively to the angle θ. It is natural for the 2D model at the very moment of delamination-onset. This is, however, not the case in 3D FEM approach, where both the coupling and the anticlastic effect come to play, even though the values of G_T are averaged along delamination front.

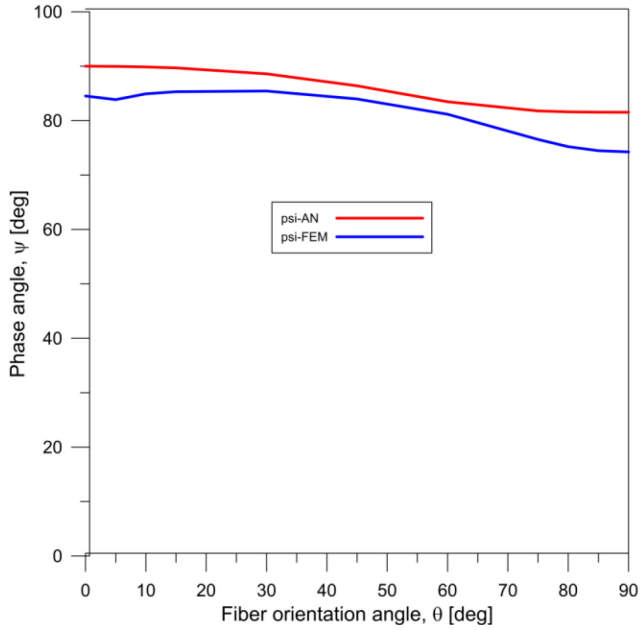

FIGURE 4. Variability of phase angle at delamination-onset for the ELS laminated beam with bending-extension coupling

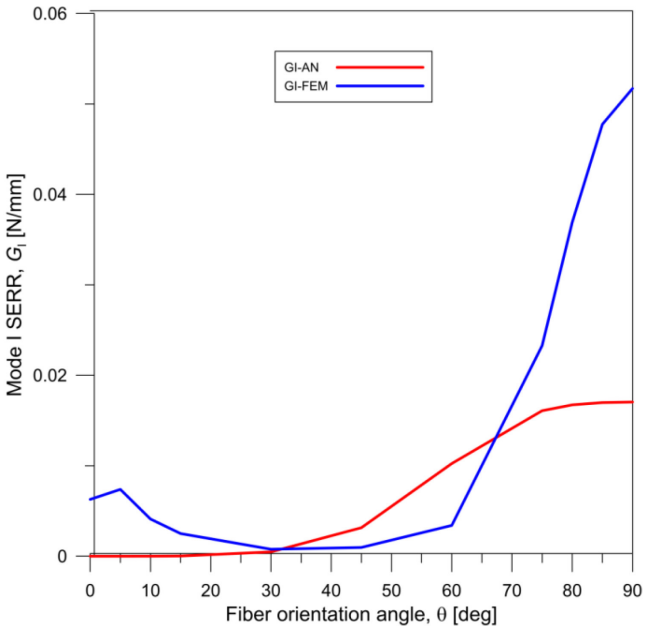

FIGURE 5. Variability of G_I at delamination-onset for the ELS laminated beam with bending-extension coupling

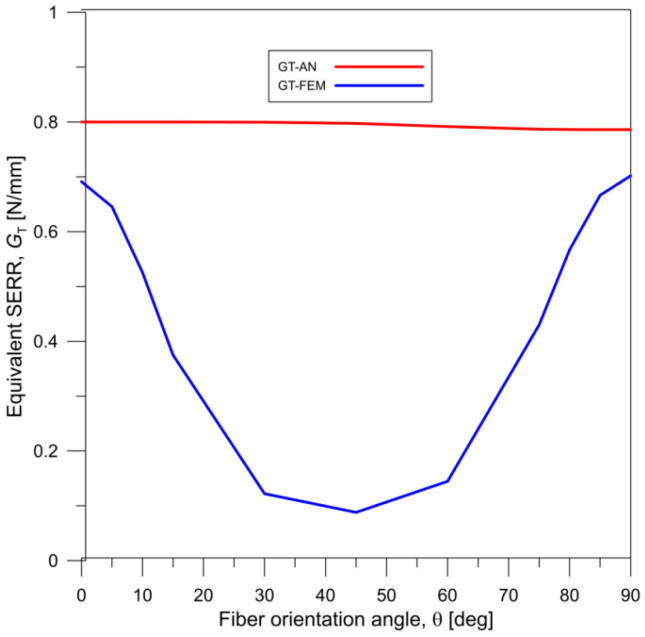

FIGURE 6. Differences in 2D and 3D approaches reflected by the total SERR vs. fiber orientation angle for the ELS laminated beam with bending-extension coupling

SUMMARY

The results obtained numerically and analytically for the ELS configuration for multi-directional coupled laminates show dependence of the deflections and SERR distribution on several factors. The most important is the type of coupling, reflected by one of the six forms of the matrix **B**. The intensity of perturbation compared to an uncoupled laminate depends on the values of fiber orientation angles in the stacking sequence. Unexpected occurrence of fracture modes I and III in the ELS test setup designed to provide pure mode II in the case of UD laminated specimens was also observed. These outcomes are in agreement with the results obtained in the ENF study [10]. The analytical results showed a good matching with the numerical ones, thus demonstrating that a simplified modelling approach is feasible for test design and experimental data reduction. Even better agreement between numerical and analytical results could be obtained by accounting for the deformability of the interface in the analytical model [19]. Besides, the numerical results based on the virtual crack closure technique could be improved by considering the corrections stemming from crack asymmetry [20, 21]. Such issues will be the subject of future investigations.

ACKNOWLEDGMENTS

The paper was financially supported by the Ministerial Research Project No. DEC-2016/21/B/ST8/03160 financed by the Polish National Science Centre.

REFERENCES

1. L. Zhao, Y. Gong, J. Zhang, Y. Chen and B. Fei, Compos. Struct. **116**, 509–522 (2014).
2. M. Bishara, M. Vogler and R. Rolfes, Compos. Struct. **169**, 116–128 (2017).
3. T. A. Sebaey, N. Blanco, J. Costa and C. S. Lopes, Compos. Sci. Technol. **72**, 1251–1256 (2012).

4. C. B. York, J. Aerosp. Eng. **23,** 219–242 (2010).
5. C. B. York, Compos. Part A **44**, 140–148 (2013).
6. H. Debski, A. Teter, T. Kubiak and S. Samborski, Compos. Struct. **136**, 593–601 (2016).
7. T. Kubiak, S. Samborski and A. Teter, Compos. Struct. **133**, 921–929 (2015).
8. A. Teter, H. Debski and S. Samborski, Thin-Walled Struct. **85**, 324–331 (2014).
9. S. Samborski, Compos. Struct. **152**, 477–487 (2016).
10. S. Samborski, Compos. Struct. **163**, 342–349 (2017).
11. ISO Standard 15114:2014.
12. P. S. Valvo, Eng. Fract. Mech. **165**, 114–139 (2016).
13. R. M. Jones, *Mechanics of composite materials* (Taylor & Francis Inc., Philadelphia, PA, 1999).
14. V. Burlayenko and T. Sadowski, Bud. i Arch. **2**, 95–109 (2008).
15. Abaqus/CAE User's Manual 6.11, Dassault Systémes, 2011.
16. M. L. Benzeggagh and M. Kenane, Compos. Sci. Technol. **56**, 439–449 (1996).
17. R. Krueger, Num. M. of Failure in Adv. Comp. Mat., 3–53 (2015).
18. P. S. Valvo, "Fracture mode partition in delaminated beams using the crack-tip displacement rates", in 18th European Conference on Fracture: Fracture of materials and structures from micro to macro scale; 30 Aug–3 Sept 2010; Dresden, Germany.
19. S. Bennati, P. Fisicaro, T. Taglialegne and P. S. Valvo, Int. J. Solids Struct. (in print).
20. P. S. Valvo, Int. J. Fract. **173**, 1–20 (2012).
21. P. S. Valvo, Int. J. Fract. **192**, 235–244 (2016).